Available online at www.sciencedirect.com
ScienceDirect
Journal of Molecular Spectroscopy 239 (2006) 160–173
Journal of MOLECULAR SPECTROSCOPY
www.elsevier.com/locate/jms

Rotation–vibration energy level clustering in the $\widetilde{X}^2B_1$ ground electronic state of PH_2

S.N. Yurchenko [a,*], W. Thiel [a], Per Jensen [b], P.R. Bunker [c]

[a] Max-Planck-Institut für Kohlenforschung, Kaiser-Wilhelm-Platz 1, D-45470 Mülheim an der Ruhr, Germany
[b] FB C—Mathematik und Naturwissenschaften, Fachgruppe Chemie, Bergische Universität Wuppertal, D-42097 Wuppertal, Germany
[c] Steacie Institute for Molecular Sciences, National Research Council of Canada, Ottawa, Ont., Canada K1A 0R6

Received 12 May 2006; in revised form 15 June 2006
Available online 15 July 2006

Abstract

We use previously determined potential energy surfaces for the Renner-coupled $\widetilde{X}^2B_1$ and $\widetilde{A}^2A_1$ electronic states of the phosphino (PH_2) free radical in a calculation of the energies and wavefunctions of highly excited rotational and vibrational energy levels of the $\widetilde{X}$ state. We show how spin–orbit coupling, the Renner effect, rotational excitation, and vibrational excitation affect the clustered energy level patterns that occur. We consider both 4-fold rotational energy level clustering caused by centrifugal distortion, and vibrational energy level pairing caused by local mode behaviour. We also calculate *ab initio* dipole moment surfaces for the $\widetilde{X}$ and $\widetilde{A}$ states, and the $\widetilde{X}$–$\widetilde{A}$ transition moment surface, in order to obtain spectral intensities.

Keywords: Phosphino; Renner; Local mode; Ab initio; Dipole moment; Intensity

1. Introduction

Analytical expressions for the potential energy surfaces of the $\widetilde{X}^2B_1$ and $\widetilde{A}^2A_1$ electronic states of the phosphino (PH_2) free radical were obtained in a recent dispersed fluorescence and *ab initio* investigation [1]. The details of how these potentials were obtained, and a discussion of previous experimental and theoretical studies on PH_2, are given in Ref. [1]. Using these potentials, the $\widetilde{X}$ state has a $\mathbf{C}_{2v}$ equilibrium structure with bond length $r_e = 1.418$ Å and bond angle $\alpha_e = 91.7°$; the $\widetilde{A}$ state has a $\mathbf{C}_{2v}$ equilibrium structure with $r_e = 1.394$ Å and $\alpha_e = 121.7°$; the barrier to linearity is 24 911.8 cm^{-1} in the $\widetilde{X}$ state and 6 686.3 cm^{-1} in the $\widetilde{A}$ state; and $T_e(\widetilde{A}) = 18225.5$ cm^{-1}. Particular interest attaches to these two states since they become degenerate as a $^2\Pi_u$ state at linearity (see Fig. 1). As a result, they are subject to the Renner effect described, for example, in Ref. [2] and in chapters 15 and 16 of Ref. [3].

In the present paper, we use the potential energy surfaces from Ref. [1] in the computer program RENNER [4–6] to calculate rotational energies for $\widetilde{X}$-state PH_2 at high angular momentum (when the rovibronic angular momentum quantum number $N \simeq 30$) in order to determine the extent of the rotational energy level clustering. Previous studies of rotational energy level clustering in triatomic molecules have concerned singlet states that are not subject to the Renner effect (see, for example, Refs. [7–10] and the references therein). We use PH_2 as an example in order to study how spin–orbit coupling and the Renner effect alter the clustering in the $\widetilde{X}$ state. We also consider, for the $\widetilde{X}$ state, the effect on the cluster formation when the stretching and bending vibrational modes are excited, and investigate the local mode character [11] of excited stretching states. For the purpose of predicting spectral intensities we calculate *ab initio* the dipole moment surfaces of the $\widetilde{X}$ and $\widetilde{A}$ states, and the $\widetilde{X}$–$\widetilde{A}$ transition moment surface.

In low angular momentum states the rotational energy level pattern for an XH_2 molecule is essentially that of a rigid asymmetric top molecule and, in particular, the four highest energies for a given value of N form two

* Corresponding author. Fax: +49 208 306 2996.
E-mail address: yurchenko@mpi-muelheim.mpg.de (S.N. Yurchenko).

0022-2852/$ - see front matter © 2006 Elsevier Inc. All rights reserved.
doi:10.1016/j.jms.2006.07.002

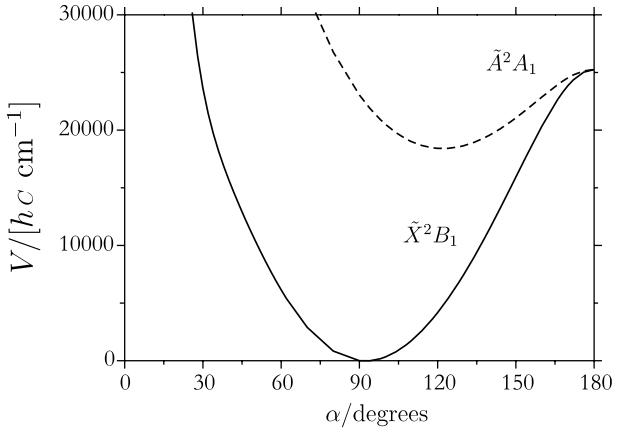

Fig. 1. The $\widetilde{X}$ and $\widetilde{A}$ potential energy curves of PH_2 as a function of the bond angle α (from Ref. [1]). The bond lengths are fixed at 1.4 Å.

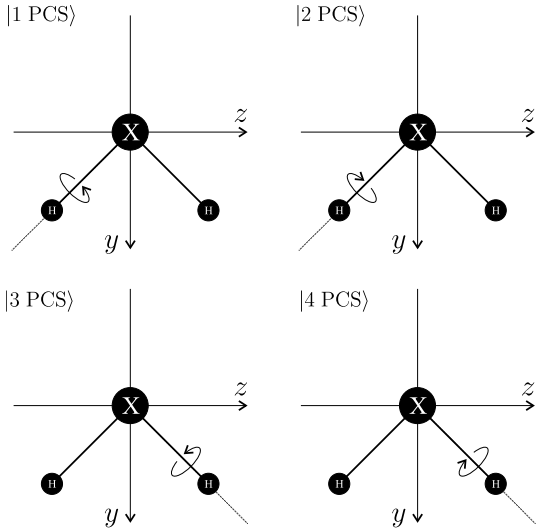

Fig. 2. The four localized *Primitive Cluster States* occurring at highest energy in an N multiplet for an ideal XH_2 molecule at high angular momentum.

K-doublets whose energy separation increases with N. However, at high N these two doublets can move close together to form a 4-fold cluster (see, for example, Fig. 2 of Ref. [8]). XH_2 molecules that have a heavy central atom X, little intermode coupling, and a bond angle close to 90°, are ideal cases for such 4-fold rotational energy level clusters to form, and these same three requirements also lead to local mode behaviour for the stretching vibrational states. Thus, PH_2 in its $\widetilde{X}$ state is a good candidate for studying both phenomena. Classically, the formation of 4-fold clusters for XH_2 molecules corresponds to the possibility being realized in high angular momentum states for there to be stable right- and left-handed rotation about each of two equivalent rotational axes, and in the ideal case these axes are aligned with the XH bonds as shown in Fig. 2. The subject of 4-fold energy level clustering in XH_2 molecules is reviewed in Ref. [10], and the interrelation with local mode vibration is described for such molecules in Ref. [11].

Semiclassical theory [7] predicts that in the ideal case 4-fold rotational energy level clustering will begin to form when N exceeds the critical value N_{cr} given by

$$N_{\mathrm{cr}} = \frac{v_2}{4A}\sqrt{\frac{A-B}{C}}, \tag{1}$$

where v_2 is the wavenumber of the bending mode, and A, B, and C are the rotational constants in cm^{-1}. For the $\widetilde{X}$ state of PH_2 using the experimental values [12] of v_2, A, B, and C, we have $N_{\mathrm{cr}} \simeq 15$. Divergence from the ideal case arises because of the finite mass of the central atom, deviation of the bond angle from 90°, and from the presence of intermode coupling; these effects shift the cluster formation to higher N values. The present paper evaluates further effects on the cluster formation that arise from the presence of electronic angular momentum and vibrational excitation for the $\widetilde{X}$ state of PH_2. We do not consider the possibility of rotational energy level clustering in the $\widetilde{A}$ state since its equilibrium bond angle is far from 90°.

2. The potential energy and dipole moment surfaces

The lower ($\widetilde{X}$) and upper ($\widetilde{A}$) potential energy surfaces, $V_-(\Delta r_{12}, \Delta r_{32}, \bar{\rho})$ and $V_+(\Delta r_{12}, \Delta r_{32}, \bar{\rho})$, respectively, are written

$$\begin{aligned} V_\pm(\Delta r_{12}, \Delta r_{32}, \bar{\rho}) &= V_0^{(\pm)}(\bar{\rho}) + \sum_j F_j^{(\pm)}(\bar{\rho}) y_j + \sum_{j\leqslant k} F_{jk}^{(\pm)}(\bar{\rho}) y_j y_k \\ &\quad + \sum_{j\leqslant k\leqslant m} F_{jkm}^{(\pm)}(\bar{\rho}) y_j y_k y_m + \sum_{j\leqslant k\leqslant m\leqslant n} F_{jkmn}^{(\pm)}(\bar{\rho}) y_j y_k y_m y_n, \end{aligned} \tag{2}$$

with

$$y_j = 1 - \exp(-a_1 \Delta r_{j2}), \tag{3}$$

$$F_{jk\ldots}^{(\pm)}(\bar{\rho}) = f_{jk\ldots}^{(0)} + \sum_{i=1}^{N} f_{jk\ldots}^{(i,\pm)} (1-\cos\bar{\rho})^i, \tag{4}$$

and

$$V_0^{(\pm)}(\bar{\rho}) = \sum_{i=1}^{8} f_0^{(i,\pm)} (1-\cos\bar{\rho})^i. \tag{5}$$

In Eq. (2), $\bar{\rho}$ is the instantaneous value of the bond angle supplement (see Figs. 15–14 of Ref. [13]), and $\Delta r_{j2} = r_{j2} - r^{(\mathrm{ref})}$, where the r_{j2} are the instantaneous P–H_j bond lengths and $r^{(\mathrm{ref})}$ is the reference value of these quantities, which is taken as the optimum bond lengths at linearity; the indices j, k, m, and n can each be 1 or 3. In Eq. (3), a_1 is a molecular parameter. In Eq. (4), the parameters $f_{jk\ldots}^{(0)}$ are common for the two potential energy surfaces and this ensures that the functions are degenerate at linearity when $\bar{\rho} = 0$; the function $F_j^{(\pm)}(\bar{\rho})$ has $N = 4$, $F_{jk}^{(\pm)}(\bar{\rho})$ has $N = 3$, $F_{jkl}^{(\pm)}(\bar{\rho})$ has $N = 2$, and $F_{jklm}^{(\pm)}(\bar{\rho})$ has $N = 1$. The adjustable parameters $f_{\ldots}^{()}$ in V_- and V_+ are constrained to ensure that V_- and V_+ are totally symmetric under the interchange of Δr_{12} and Δr_{32} which they must be for a symmetrical molecule like PH_2.

Table 1
The non-zero potential energy parameters[a] from Ref. [1] for the $\widetilde{X}\,^2B_1$ and $\widetilde{A}\,^2A_1$ states of PH_2 [see Eqs. (2)–(5)]

$r^{(\mathrm{ref})}$ (Å)	1.386178	
a_1 (Å^{-1})	1.7947	
$f_{11}^{(0)}$	29428	
$f_{13}^{(0)}$	−2286	
$f_{111}^{(0)}$	1564	
$f_{113}^{(0)}$	−1043	
$f_{1111}^{(0)}$	2940	
$f_{1113}^{(0)}$	1488	
$f_{1133}^{(0)}$	1808	
	$\widetilde{X}^2B_1(\sigma=-)$	$\widetilde{A}^2A_1(\sigma=+)$
$f_0^{(1,\sigma)}$	−80123	−42568
$f_0^{(2,\sigma)}$	128819	121348
$f_0^{(3,\sigma)}$	−145465	−225373
$f_0^{(4,\sigma)}$	106891	279870
$f_0^{(5,\sigma)}$	−41711	−187027
$f_0^{(6,\sigma)}$	6884	51721
$f_1^{(1,\sigma)}$	−15978	−4311
$f_1^{(2,\sigma)}$	30271	11646
$f_1^{(3,\sigma)}$	−23204	−15736
$f_1^{(4,\sigma)}$	5602	6095
$f_{11}^{(1,\sigma)}$	−6470	−239
$f_{11}^{(2,\sigma)}$	11563	3022
$f_{11}^{(3,\sigma)}$	−5798	−3965
$f_{13}^{(1,\sigma)}$	2899	3454
$f_{13}^{(2,\sigma)}$	−2141	−3492
$f_{13}^{(3,\sigma)}$	1505	2761
$f_{111}^{(1,\sigma)}$	1189	1685
$f_{111}^{(2,\sigma)}$	−477	−2302
$f_{113}^{(2,\sigma)}$	924	241
$f_{1111}^{(1,\sigma)}$		−3584
$f_{1113}^{(1,\sigma)}$	−1424	−4225
$f_{1133}^{(1,\sigma)}$	−816	−4818

[a] Units are cm^{-1} unless otherwise indicated.

The values of these parameters, as determined in Ref. [1], are given in Table 1. We use these parameters, with the spin–orbit coupling parameter $A_{\mathrm{SO}} = 200\ \mathrm{cm}^{-1}$ as in Ref. [1] (see Ref. [14]), in the RENNER program [6] to calculate rovibronic energies and wavefunctions. We have calculated rovibronic energies up to $J = 61/2$ so that we have both F_1 and F_2 energies for states up to $N = 30$. The angular momentum quantum number J is used for the sum of rovibronic and electron spin angular momenta. For a given value of N in a doublet state the level with $J = N + \frac{1}{2}$ is called the F_1 fine structure component, and the level with $J = N - \frac{1}{2}$ is called the F_2 component. The calculation was made using a Morse oscillator rigid bender basis set that had been chosen after making convergence tests for the high angular momentum states involved. For both surfaces we used the $N_{\mathrm{Bend}} = 8$ lowest bending basis functions. The stretching function basis was selected using Morse oscillator functions $|n_1 n_3\rangle$ having $n_1 + n_3 \leqslant N_{\mathrm{Stretch}} = 15$. Of these functions we used the $N_A = 6$ lowest stretching basis functions of A_1 symmetry, and the $N_B = 4$ lowest stretching basis functions of B_2 symmetry for both electronic states. This means that we included all vibrational basis states having energies below 9 500 cm^{-1}.

The expressions for the intensities of rovibronic transitions within and between two Renner-degenerate electronic states are given in Ref. [6]. To make use of the expressions, we calculated *ab initio* the μ_a and μ_b electronic dipole moment surfaces for the $\widetilde{X}$ and $\widetilde{A}$ states, and the μ_c transition moment surface between the $\widetilde{X}$ and $\widetilde{A}$ states, at several hundred nuclear configurations of the PH_2 molecule using the MOLPRO2002 computer package [15] at the multi-reference configuration-interaction (MRCI) level [16,17]. We used a aug-cc-pVTZ basis set [18] with an active space comprising seven electrons in eight molecular orbitals where the five core orbitals were frozen. The $\mathbf{C}_s$ point group was used to classify the electronic wavefunctions. The calculations were done for PH bond lengths in the range 1.12–1.6 Å for both electronic states. For the two $\widetilde{A}$ state dipole moment surfaces, and for the $\widetilde{A}$–$\widetilde{X}$ transition moment surface, we made the calculations with bond angles in the range 75°–170°. Since the potential for the $\widetilde{A}$ state goes up steeply at bond angles less than 75° it was unnecessary to perform calculations involving this state at smaller bond angles. This meant that we did not have to worry about the effect of the conical intersection of the $\widetilde{A}$ state with the $\widetilde{B}$ state which occurs at smaller bond angle. For the $\widetilde{X}$ state, we calculated its two dipole moment surfaces with bond angles in the range 40°–160°.

In the *ab initio* calculation of the dipole moments and transition moment we define three axes *xqp*, with origin in the nuclear center of mass, which are attached directly to the instantaneous nuclear configuration of the molecule (see Fig. 1 of Ref. [20]). For PH_2 at any nuclear configuration, the q axis is defined as bisecting the bond angle ∠(HPH) and is directed so that the q coordinates of the H nuclei 1 and 3 are positive. The p axis is perpendicular to the q axis in the HPH plane and its direction is such that the p coordinate of nucleus 3 is positive. The x axis is perpendicular to the molecular plane and directed so that *xqp* is right-handed.

We denote the electronic wavefunction for the $\widetilde{X}$ state as $\psi_{\mathrm{elec}}^{(-)}$ and that for the $\widetilde{A}$ state as $\psi_{\mathrm{elec}}^{(+)}$. In this notation we obtain the following non-vanishing dipole and transition moments:

$$\bar{\mu}_p^{(\sigma)}(\Delta r_{12}, \Delta r_{32}, \bar{\rho}) = \langle \psi_{\mathrm{elec}}^{(\sigma)} | \mu_p | \psi_{\mathrm{elec}}^{(\sigma)} \rangle_{\mathrm{el}}, \tag{6}$$

$$\bar{\mu}_q^{(\sigma)}(\Delta r_{12}, \Delta r_{32}, \bar{\rho}) = \langle \psi_{\mathrm{elec}}^{(\sigma)} | \mu_q | \psi_{\mathrm{elec}}^{(\sigma)} \rangle_{\mathrm{el}} \tag{7}$$

where, in Eqs. (6) and (7), $\sigma = -$ or $+$, and

$$\bar{\mu}_x^{(-+)}(\Delta r_{12},\Delta r_{32},\bar{\rho}) = \langle \psi_{\rm elec}^{(-)}|\mu_x|\psi_{\rm elec}^{(+)}\rangle_{\rm el}. \quad (8)$$

where, in Eqs. (6)–(8), the subscript 'el' indicates that integration is over the electronic coordinates only. The functions $\bar{\mu}_p^{(\sigma)}$ and $\bar{\mu}_q^{(\sigma)}$ are represented as (see Ref. [20])

$$\begin{aligned}\bar{\mu}_p^{(\sigma)}(\Delta r_{12},\Delta r_{32},\bar{\rho}) = {} & \mu_0^{(p;\sigma)}(\bar{\rho}) + \sum_j \mu_j^{(p;\sigma)}(\bar{\rho})\Delta r_{j2} \\ & + \sum_{j\leqslant k} \mu_{jk}^{(p;\sigma)}(\bar{\rho})\Delta r_{j2}\Delta r_{k2} \\ & + \sum_{j\leqslant k\leqslant m} \mu_{jkm}^{(p;\sigma)}(\bar{\rho})\Delta r_{j2}\Delta r_{k2}\Delta r_{m2} \\ & + \sum_{j\leqslant k\leqslant m\leqslant n} \mu_{jkmn}^{(p;\sigma)}(\bar{\rho})\Delta r_{j2}\Delta r_{k2}\Delta r_{m2}\Delta r_{n2}\end{aligned} \quad (9)$$

and

$$\begin{aligned}\bar{\mu}_q^{(\sigma)}(\Delta r_{12},\Delta r_{32},\bar{\rho}) = \sin\bar{\rho}\Big[& \mu_0^{(q;\sigma)}(\bar{\rho}) + \sum_j \mu_j^{(q;\sigma)}(\bar{\rho})\Delta r_{j2} \\ & + \sum_{j\leqslant k} \mu_{jk}^{(q;\sigma)}(\bar{\rho})\Delta r_{j2}\Delta r_{k2} \\ & + \sum_{j\leqslant k\leqslant m} \mu_{jkm}^{(q;\sigma)}(\bar{\rho})\Delta r_{j2}\Delta r_{k2}\Delta r_{m2} \\ & + \sum_{j\leqslant k\leqslant m\leqslant n} \mu_{jkmn}^{(q;\sigma)}(\bar{\rho})\Delta r_{j2}\Delta r_{k2}\Delta r_{m2}\Delta r_{n2}\Big],\end{aligned} \quad (10)$$

with j, k, m, $n = 1$ or 3. The angle-dependent coefficients are given by

$$\mu_{jk\ldots}^{(w;\sigma)}(\bar{\rho}) = \sum_{i=0}^{N} w_{jk\ldots}^{(i;\sigma)}(1-\cos\bar{\rho})^i, \quad (11)$$

with $w=$ p or q. The function $\mu_0^{(w;\sigma)}(\bar{\rho})$ has $N=8$, $\mu_j^{(w;\sigma)}(\bar{\rho})$ has $N=4$, $\mu_{jk}^{(w;\sigma)}(\bar{\rho})$ has $N=3$, $\mu_{jkm}^{(w;\sigma)}(\bar{\rho})$ has $N=2$ and $\mu_{jkmn}^{(w;\sigma)}(\bar{\rho})$ has $N=1$. The function $\bar{\mu}_x^{(-+)}$ is parameterized as

$$\begin{aligned}\bar{\mu}_x^{(-+)}(\Delta r_{12},\Delta r_{32},\bar{\rho}) = \sin\bar{\rho}\Big[& \mu_0^{(x;-+)}(\bar{\rho}) \\ & + \sum_j \mu_j^{(x;-+)}(\bar{\rho})\Delta r_{j2} \\ & + \sum_{j\leqslant k} \mu_{jk}^{(x;-+)}(\bar{\rho})\Delta r_{j2}\Delta r_{k2} \\ & + \sum_{j\leqslant k\leqslant m} \mu_{jkm}^{(x;-+)}(\bar{\rho})\Delta r_{j2}\Delta r_{k2}\Delta r_{m2} \\ & + \sum_{j\leqslant k\leqslant m\leqslant n} \mu_{jkmn}^{(x;-+)}(\bar{\rho})\Delta r_{j2}\Delta r_{k2}\Delta r_{m2}\Delta r_{n2}\Big],\end{aligned} \quad (12)$$

with

$$\mu_{jk\ldots}^{(x;-+)}(\bar{\rho}) = \sum_{i=0}^{N} x_{jk\ldots}^{(i;-+)}(1-\cos\bar{\rho})^i, \quad (13)$$

where the number of summation terms N is given exactly as for Eq. (11). For a symmetrical molecules like PH_2, relations exist between the expansion coefficients in Eqs. (11) and (13), so that the functions $\bar{\mu}_q^{(\sigma)}$ and $\bar{\mu}_x^{(-+)}$ are unchanged under the interchange of the two protons, whereas the function $\bar{\mu}_p^{(\sigma)}$ is anti-symmetric under this operation.

For the dipole moment and transition moment surfaces we obtain values for the $p_{jk\ldots}^{(i;\sigma)}$, $q_{jk\ldots}^{(i;\sigma)}$, and $x_{jk\ldots}^{(i;-+)}$ parameters by fitting Eqs. (9)–(13) through the *ab initio* dipole moment and transition moment values. The results of the fittings (parameter values, standard errors, and the standard deviations of the fittings) are given in Table 2.

Table 2
The *ab initio* dipole and transition moment parameters for the $\widetilde{X}$ and $\widetilde{A}$ electronic states of PH_2 [see Eqs. (9)–(13)]

	$\widetilde{X}^1A_1$		$\widetilde{A}^1B_1$
$q_0^{(0;-)}$/D	3.5060(97)[a]	$q_0^{(0;+)}$/D	1.6373(76)
$q_0^{(1;-)}$/D	−12.84(12)	$q_0^{(1;+)}$/D	−7.136(98)
$q_0^{(2;-)}$/D	32.05(52)	$q_0^{(2;+)}$/D	17.82(42)
$q_0^{(3;-)}$/D	−48.0(10)	$q_0^{(3;+)}$/D	−24.15(78)
$q_0^{(4;-)}$/D	40.35(99)	$q_0^{(4;+)}$/D	16.04(63)
$q_0^{(5;-)}$/D	−17.66(46)	$q_0^{(5;+)}$/D	−4.09(19)
$q_0^{(6;-)}$/D	3.147(84)	$q_1^{(0;+)}$/D (Å^{-1})	−0.0444(84)
$q_1^{(0;-)}$/D (Å^{-1})	−0.508(41)	$q_1^{(1;+)}$/D (Å^{-1})	0.5384(83)
$q_1^{(1;-)}$/D (Å^{-1})	−2.74(21)	$q_{11}^{(0;+)}$/D (Å^{-2})	0.396(92)
$q_1^{(2;-)}$/D (Å^{-1})	5.32(38)	$q_{13}^{(0;+)}$/D (Å^{-2})	−1.20(19)
$q_1^{(3;-)}$/D (Å^{-1})	−3.54(27)	$q_{113}^{(0;+)}$/D (Å^{-3})	−1.05(16)
$q_1^{(4;-)}$/D (Å^{-1})	0.763(67)	SD[b]/D	0.011
$q_{11}^{(0;-)}$/D (Å^{-2})	−2.26(18)		
$q_{11}^{(1;-)}$/D (Å^{-2})	3.44(30)		
$q_{11}^{(2;-)}$/D (Å^{-2})	−1.45(12)		
SD[b]/D	0.0078		
$p_1^{(0;-)}$/D (Å^{-1})	−0.617(19)	$p_1^{(0;+)}$/D (Å^{-1})	−1.0048(99)
$p_1^{(1;-)}$/D (Å^{-1})	3.040(85)	$p_1^{(1;+)}$/D (Å^{-1})	2.832(83)
$p_1^{(2;-)}$/D (Å^{-1})	−1.96(10)	$p_1^{(2;+)}$/D (Å^{-1})	−2.78(17)
$p_1^{(3;-)}$/D (Å^{-1})	0.426(36)	$p_1^{(3;+)}$/D (Å^{-1})	1.051(88)
$p_{11}^{(0;-)}$/D (Å^{-2})	1.236(54)	$p_{11}^{(0;+)}$/D (Å^{-2})	0.162(26)
$p_{11}^{(1;-)}$/D (Å^{-2})	−0.729(40)	$p_{11}^{(1;+)}$/D (Å^{-2})	−0.661(36)
SD[b]/D	0.0053	SD[b]/D	0.0060
	$\widetilde{X}/\widetilde{A}$		
$x_0^{(0;-+)}$/D	0.9226(45)	$x_1^{(2;-+)}$/D (Å^{-1})	9.32(46)
$x_0^{(1;-+)}$/D	−1.444(37)	$x_1^{(3;-+)}$/D (Å^{-1})	−8.40(51)
$x_0^{(2;-+)}$/D	2.66(10)	$x_1^{(4;-+)}$/D (Å^{-1})	2.66(19)
$x_0^{(3;-+)}$/D	−2.18(11)	$x_{11}^{(0;-+)}$/D (Å^{-2})	0.106(66)
$x_0^{(4;-+)}$/D	0.696(41)	$x_{11}^{(1;-+)}$/D (Å^{-2})	−1.06(20)
$x_1^{(0;-+)}$/D (Å^{-1})	0.437(19)	$x_{11}^{(2;-+)}$/D (Å^{-2})	0.65(14)
$x_1^{(1;-+)}$/D (Å^{-1})	−4.37(16)	$x_{111}^{(0;-+)}$/D (Å^{-3})	−0.42(13)
		SD[b]/D	0.0077

[a] Quantities in parentheses are standard errors in units of the last digit quoted.
[b] Standard deviation of the fitting to the *ab initio* points.

From the *ab initio* calculation we determine that the dipole moment for the $\widetilde{X}$ state at its equilibrium configuration is 0.57 D, and for the $\widetilde{A}$ state at its equilibrium configuration it is 0.34 D. In an earlier configuration interaction (CISD) study [19] values of 0.57 D and 0.36 D were obtained for these equilibrium dipole moments.

The $\widetilde{A}$–$\widetilde{X}$ transition moment μ_c at the equilibrium geometry of the $\widetilde{X}$ state is calculated to be 0.63 D. This corresponds to a radiative lifetime of about 10^{-6} s which agrees with what is found experimentally [22,23]. The angular dependence of the electronic transition moment integral, Eq. (8), between the $\widetilde{A}$ and $\widetilde{X}$ states of PH_2 has been previously obtained in an *ab initio* MRCI calculation [21] for bond lengths fixed at 1.418 Å, and the results are plotted at the bottom of Fig. 1 in Ref. [21]. The values given in this figure are about a factor of 7.5 smaller than the transition moments that we obtain, but the variation with bending angle is very similar to our result. The fact that our result is in accord with the lifetime measurements [22,23] leads us to suspect that there is some trivial error, most probably in the ordinate units, of the transition moment plot of Ref. [21].

3. Four-fold energy level clusters in the $\widetilde{X}$ state

The calculated rovibronic term values for the ground vibronic state of PH_2 are shown in Fig. 3, where the term values are plotted relative to the highest term value for each N. A magnified view of the top is shown in the right-hand part of the figure. On the scales to which the two parts of the figure are drawn, the K-doubling is mostly not resolved, in which case each term represents two levels. We see that the top cluster begins to form as N increases above 15, in accordance with Eq. (1). In Table 3, the top eight $N = 30$ term values are given in the left-most column (for $A_{SO} = 200\ cm^{-1}$ and $T_e(\widetilde{A}) = 18\,225.5\ cm^{-1}$). The clustering pattern in Fig. 3 is similar to that obtained for certain XH_2 molecules in singlet states (see, for example, Figs. 2 and 3 in [8]). For singlet states $J \equiv N$ and the top four levels for each J move closer and closer together as J is increased above J_{cr}. For doublet states the top four F_1 levels move closer together as N is increased above N_{cr} as do the top four F_2 levels. At very high N for ground vibronic state PH_2, this produces two 4-fold rotational energy level clusters: a higher 4-fold cluster of F_1 levels and a lower 4-fold cluster of F_2 levels. If there were no spin–orbit coupling

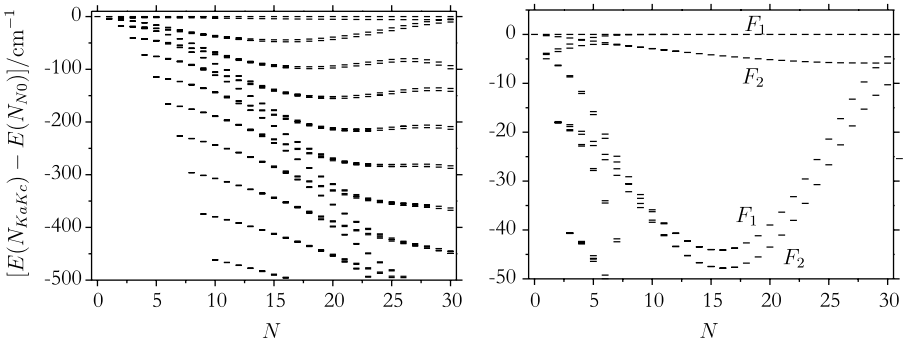

Fig. 3. The rotational term values for PH_2 in its ground vibronic state ($T_e(\widetilde{A}) = 18225.5\ cm^{-1}$ and $A_{SO} = 200\ cm^{-1}$) plotted relative to the highest term value for each N. In the magnified view on the right, only the top levels are shown, and the F_1 and F_2 spin fine structure components are indicated.

Table 3
Term values (in cm^{-1}) of the top four $F_1(N_{K_aK_c})$ and top four $F_2(N_{K_aK_c})$ levels for $N = 30$, in the ground vibronic state of PH_2, as a function of A_{SO} and $T_e(\widetilde{A})$ (see text); $\delta_{cluster}$ is the cluster splitting, and $\Delta_{spin}(30_{30,0})$ is the spin splitting in the $30_{30,0}$ level

A_{SO} (cm^{-1})	200	400	800	200	200	200	200
$T_e(\widetilde{A})$ (cm^{-1})	18225.5	18225.5	18225.5	10000	5000	2500	1000
$J = 61/2$ (F_1 levels)							
$30_{30,0}$	7579.795	7583.874	7594.418	7574.097	7563.803	7545.302	7502.181
$30_{30,1}$	7579.795	7583.874	7594.418	7574.097	7563.803	7545.303	7502.181
$30_{29,1}$	7575.224	7579.212	7589.528	7569.546	7559.307	7540.913	7498.215
$30_{29,2}$	7575.224	7579.212	7589.528	7569.546	7559.307	7540.913	7498.215
$\delta_{cluster}(F_1)$	4.57	4.66	4.89	4.55	4.50	4.39	3.97
$J = 59/2$ (F_2 levels)							
$30_{30,0}$	7573.927	7572.161	7571.079	7561.089	7537.614	7496.755	7412.466
$30_{30,1}$	7573.927	7572.161	7571.079	7561.089	7537.614	7496.755	7412.466
$30_{29,1}$	7569.501	7567.794	7566.798	7556.840	7533.756	7493.626	7410.735
$30_{29,2}$	7569.501	7567.794	7566.798	7556.840	7533.756	7493.626	7410.735
$\delta_{cluster}(F_2)$	4.43	4.37	4.28	4.25	3.86	3.13	1.73
$\Delta_{spin}(30_{30,0})$	5.87	11.71	23.34	13.01	26.19	48.55	89.72

(i.e., if A_{SO} were zero or if $T_0(\widetilde{A})$ were infinite) then there would be no spin splitting between the F_1 and F_2 levels and an 8-fold energy level cluster would form. Since both $T_0(\widetilde{A})$ and the barrier to linearity in the ground state are very high in comparison to the lower state term values considered here, the effects of both the electronic correction to the A rotational constant, and to the effective spin–rotation constant ϵ_{aa}, can be calculated using second-order perturbation theory [24]. This was done in the original analyses of the PH_2 spectrum [25,26]. The present approach is far more complete, and confirms that such small coupling terms do not have a drastic effect on the rotational term value patterns.

To analyze the clustering further in the ground vibronic state of PH_2, we have made calculations with the spin–orbit coupling constant A_{SO} changed from 200 to 400 and 800 cm^{-1}, and we have also changed $T_e(\widetilde{A})$ from 18 225.5 to 10 000, 5000, 2500, and 1000 cm^{-1}. The $\widetilde{A}$-state potential surface was modified to give these latter four $T_e(\widetilde{A})$ values by changing $f_0^{(1,+)}$ from −42 568 to −54 987.5, −60 353.6, −62 827.6, and −64 271.3 cm^{-1}, respectively. The resultant term values are plotted in Fig. 4 for each of the six cases, and tabulated for the top four F_1 and F_2 levels having $N = 30$ in Table 3. This shows how spin–orbit coupling and the Renner effect influence the cluster splitting and the spin splitting. H_2S^+ and AsH_2 have spin–orbit coupling constants of about 400 and 1500 cm^{-1}, respectively, and they thus provide experimental tests for the effect of increasing the spin–orbit coupling. However, the study of energy level clustering in these molecules is best dealt with in a separate publication. Decreasing $T_e(\widetilde{A})$ increases the effect of both spin–orbit coupling and the Renner effect since it moves coupled levels closer together. We see that the F_1–F_2 spin splitting in the topmost 8-fold cluster is proportional to A_{SO} and inversely proportional to $T_e(\widetilde{A})$. On the other hand the magnitude of the F_1 and F_2 cluster splittings in the topmost cluster is largely unaffected by either of these interactions except when $T_e(\widetilde{A})$ is less than the bending wavenumber. In this latter case there will be near resonances between Renner-coupled rovibrational states and

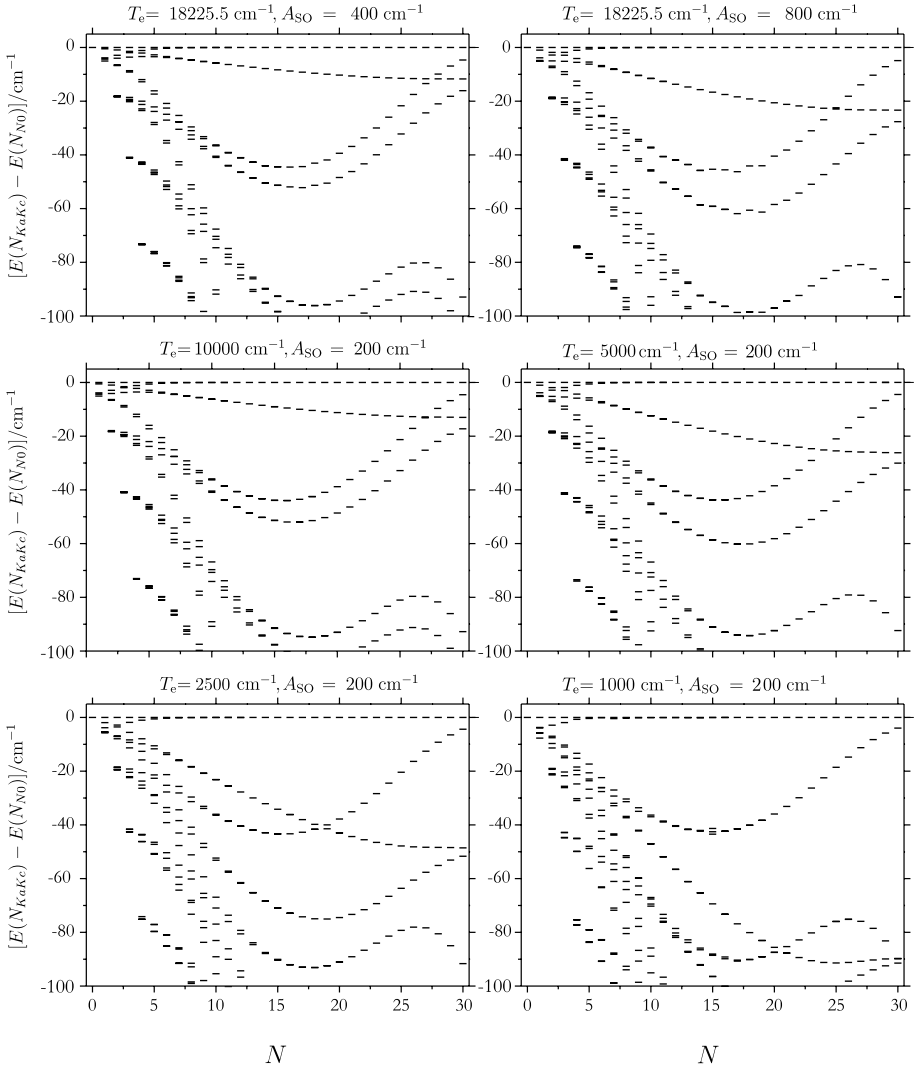

Fig. 4. The dependence of the cluster splittings on A_{SO} and $T_e(\widetilde{A})$ for PH_2 in its ground vibronic state.

Table 4
Term values (in cm^{-1}) of the top four $F_1(N_{K_aK_c})$ and top four $F_2(N_{K_aK_c})$ levels for $N = 30$, in the $\widetilde{X}$ state of PH_2, as a function of v_2; $\delta_{cluster}$ is the cluster splitting, and $\Delta_{spin}(30_{30,0})$ is the spin splitting in the $30_{30,0}$ level

v_2	0	1	2	3	4	5	6
$J = 61/2$ (F_1 levels)							
$30_{30,0}$	7579.795	8823.019	10060.467	11293.747	12524.256	13754.033	14996.432
$30_{30,1}$	7579.795	8823.019	10060.467	11293.747	12524.256	13754.033	14996.453
$30_{29,1}$	7575.224	8819.117	10057.135	11290.928	12521.913	13752.170	14995.450
$30_{29,2}$	7575.224	8819.117	10057.135	11290.928	12521.913	13752.169	14995.426
$\delta_{cluster}(F_1)$	4.57	3.90	3.33	2.82	2.34	1.86	1.03
$J = 59/2$ (F_2 levels)							
$30_{30,0}$	7573.927	8817.095	10054.422	11287.535	12517.901	13747.543	14990.002
$30_{30,1}$	7573.927	8817.095	10054.422	11287.535	12517.901	13747.543	14990.003
$30_{29,1}$	7569.501	8813.309	10051.189	11284.798	12515.623	13745.729	14989.021
$30_{29,2}$	7569.501	8813.319	10051.189	11284.798	12515.623	13745.730	14988.999
$\delta_{cluster}(F_2)$	4.43	3.79	3.23	2.74	2.28	1.81	1.00
$\Delta_{spin}(30_{30,0})$	5.87	5.92	6.05	6.21	6.36	6.49	6.43

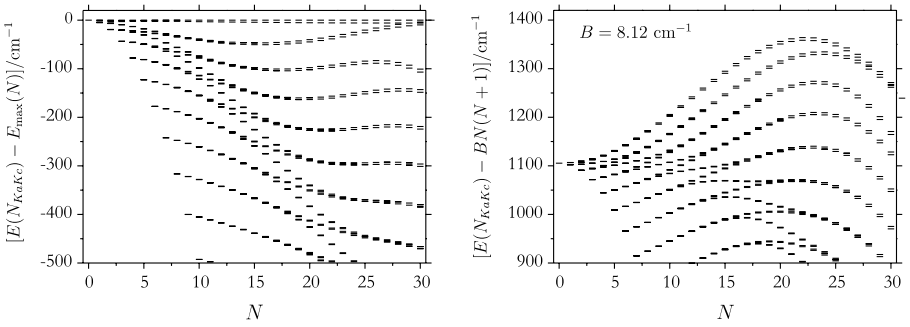

Fig. 5. Two presentations of the 4-fold cluster formation in the $v_2 = 1$ state.

this will cause significant changes in the spin–orbit splittings and rotational energy level separations.

The effect of bending excitation on cluster formation (with $v_2 = 0$, 1 or 2) in the (singlet) ground electronic state of H_2Se has already been studied [8,9]. Here, we pursue this further for the doublet ground state of PH_2. In Table 4 we list the term values of the top four $F_1(N_{K_aK_c})$ and top four $F_2(N_{K_aK_c})$ levels for $N = 30$, in the $\widetilde{X}$ state of PH_2, for v_2 values of 0–6. We see that bending vibrational excitation has a rather small effect on the spin splitting, increasing it by 9.5% as v_2 changes from 0 to 6. However, this increase in the bending quantum number causes a decrease by more than a factor of four in both the F_1 and F_2 cluster splittings. Two ways of plotting the cluster formation for the $v_2 = 1$ state are given in Fig. 5. In the right-hand plot $BN(N+1)$ is subtracted (with B taken as 8.12 cm^{-1}); this way of plotting the data allows one to appreciate the term values of the levels.

In the above discussion of rotational energy level cluster formation in excited bending states the possible influence of excited stretching states has been neglected. It turns out that this is justified since at the high N values where clustering occurs such influence is negligible for $\widetilde{X}$-state PH_2. We consider the situation for the $v_1/v_3/2v_2$ polyad of levels; 4-fold energy level clustering in this polyad for the H_2Se molecule has been discussed in Ref. [9] (see Figs. 3 and 4 of Ref. [9]). For $\widetilde{X}$-state PH_2 we calculate the term values for the $(N,J) = (0,1/2)$ level of the v_1, v_3 and $2v_2$ states as 2309.2, 2314.3, and 2197.4 cm^{-1}, respectively, whereas for the topmost (30,61/2) level, the v_1, v_3, and $2v_2$ rovibronic term values are 9864.1, 9672.5, and 10 060.5 cm^{-1}, respectively. The rotational constants of the $2v_2$ state are larger than those of the v_1 or v_3 states so that as N increases the levels of the $2v_2$ state approach those of the stretching states, cross them,[1] and then move above them; the N value of closest approach is 13, which is well below the N value at which there is significant 4-fold energy level clustering. In Fig. 6 we show the rotation–vibration term values calculated for $\widetilde{X}$-state PH_2 in the $v_1/v_3/2v_2$ region, plotted with subtraction of $BN(N+1)$, as a function of N. In this figure the topmost $N = 30$ levels for v_1, v_3, and $2v_2$ occur at 2312.5, 2120.9, and 2508.9 cm^{-1} after subtracting $BN(N+1)$ with $B = 8.12$ cm^{-1}.

4. Local mode behaviour

In Fig. 7 we show the correlation diagram for the lowest 10 stretching vibrational term values of an XH_2 molecule

[1] Strictly speaking the v_1 (or v_3) and $2v_2$ levels of the same symmetry and J value will avoid crossing.

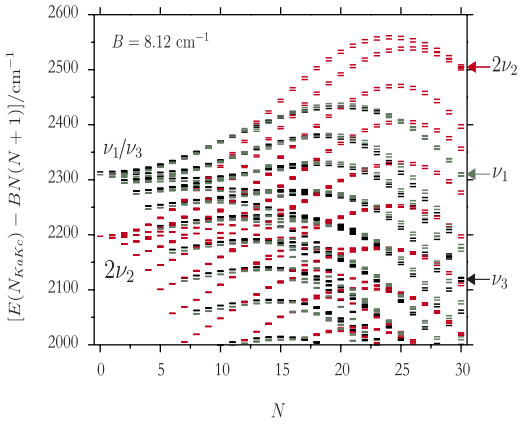

Fig. 6. Four-fold clustering in the $\nu_1/\nu_3/2\nu_2$ region. The position of the highest $N = 30$ level in each of the three vibrational states is indicated at the right.

between (on the left) the harmonic oscillator normal mode limit, and (on the right) the local mode limit. In the harmonic oscillator limit the term values are given by

$$G(v_1, v_3) = \left(v_1 + \tfrac{1}{2}\right)\omega_1 + \left(v_3 + \tfrac{1}{2}\right)\omega_3 = (v_1 + v_3 + 1)(\omega_1 + \omega_3)/2 + (v_1 - v_3)(\omega_1 - \omega_3)/2, \quad (14)$$

where ω_1 and ω_3 are the harmonic wavenumbers, and v_1 and v_3 are the harmonic oscillator quantum numbers for the symmetric (A_1) and anti-symmetric (B_2) stretching vibrational normal modes, respectively. In the local mode limit the term values are given by

$$G(m,n) = \left(m + \frac{1}{2}\right)\omega_M + \left(m + \frac{1}{2}\right)^2 x_M + \left(n + \frac{1}{2}\right)\omega_M + \left(n + \frac{1}{2}\right)^2 x_M = (m + n + 1)\omega_M + [(m + n + 1)^2 + (n - m)^2]x_M/2, \quad (15)$$

where $\omega_M > 0$ and $x_M < 0$ are the harmonic wavenumber and anharmonicity constant of an X–H bond treated as a Morse oscillator, and m and n are the bond vibration quantum numbers. On either side of the diagram the stretching term values occur as manifolds containing $(v_1 + v_3 + 1) = (m + n + 1) = V + 1$ members, where V indicates the degree of stretching excitation. In the normal mode limit the levels within a manifold are evenly spaced, whereas in the local mode limit they pair up because $G(m,n) = G(n,m)$ for $n \neq m$. The pair at lowest energy has $(m,n) = (V,0)$ and $(0,V)$ since for them $(n - m)^2$ is a maximum ($x_M < 0$). For V even, there is one 'lonely' level with $(m,n) = (V/2, V/2)$ at the highest energy while for V odd, the pair with $(m,n) = ((V + 1)/2, (V - 1)/2)$ and $((V - 1)/2, (V + 1)/2)$ are at the highest energy.

Local mode vibrations have been the subject of much research and a recent review [11] provides an introduction to the theory; it also references earlier reviews and research papers on the subject.

For an XH_2 molecule, the eigenfunctions of the stretching Hamiltonian must transform irreducibly in $\mathbf{C}_{2v}$ If we let $|mn\rangle$ denote a local mode wavefunction with m quanta in the r_{12} oscillator and n quanta in r_{32}, then we form symmetrized normalized wavefunctions as

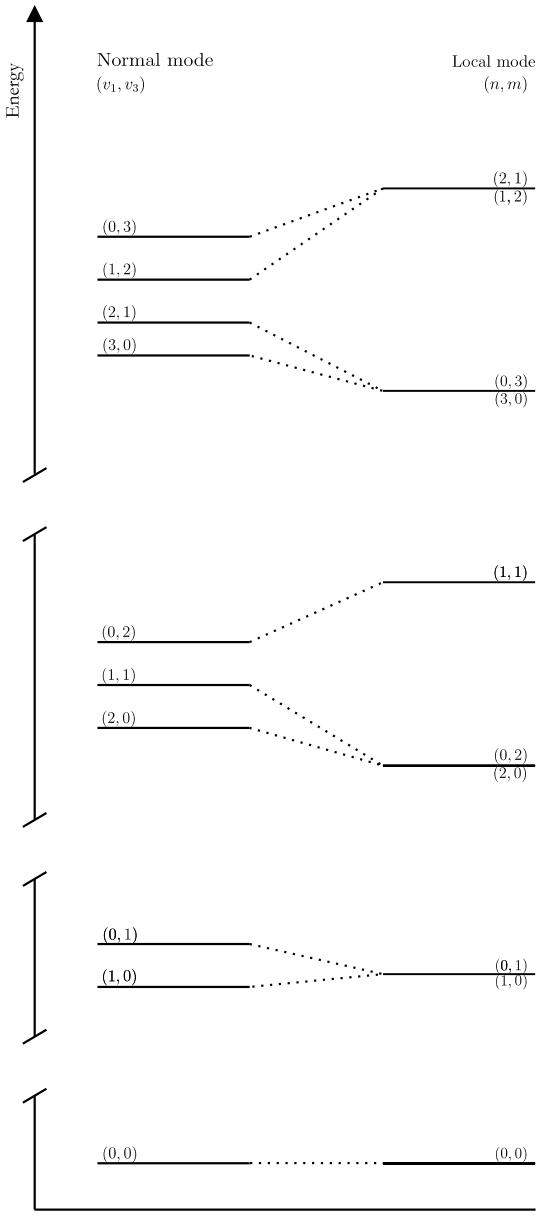

Fig. 7. A schematic representation of the stretching vibrational term values of an XH_2 molecule with the harmonic normal mode energy level pattern on the left (assuming $\omega_3 > \omega_1$) and the pure local mode energy level pattern on the right; see Eqs. (14) and (15).

$$|mn^{\pm}\rangle = [|mn\rangle \pm |nm\rangle]/\sqrt{2}, \quad (16)$$

where the + combination is of A_1 symmetry and the − combination is B_2. In local mode notation symmetrized stretching states are denoted $(mn^{\pm})$ with $m \geqslant n$. States of B_2 symmetry must have $m \neq n$.

To study the local mode behaviour of highly excited vibrational states of $\widetilde{X}$-state PH_2, we made an $N = 0$, $J = 1/2$ calculation using the computer program RENNER, with the potentials of Table 1 and $A_{SO} = 200\ \text{cm}^{-1}$, in which we included all basis states having vibrational term values up to $15\,500\ \text{cm}^{-1}$. To do this we used a basis set with $N_{Bend} = 13(14)$, $N_{Stretch} = 20(20)$, $N_A = 15(13)$, and $N_B = 12(10)$ for the $\widetilde{X}(\widetilde{A})$ state. As a result, all vibrational term val-

ues up to at least 10 000 cm^{-1} are converged. The results show that the vibrational energy level manifolds for the stretching vibrational states of PH_2 in its $\widetilde{X}$ state have near-degenerate pairs of energy levels, and they conform closely to the local mode energy level pattern. The results also show how bending vibrational excitation affects the situation.

In Table 5, under the heading RENNER, we give the lowest ten stretching vibrational term values that we obtain, relative to the lowest one, for each of the four bending states $v_2 = 0$, 1, 2, and 3, where v_2 is the harmonic oscillator bending quantum number. In each of the four cases the pattern is close to that of a pure local mode oscillator. As explained, for example, in Ref. [11], in order to approximately account for interactions between the two bond stretches in the local mode Hamiltonian, we use the harmonically coupled anharmonic oscillator (HCAO) model [27,28] in which diagonal matrix elements are given by Eq. (15) and the only non-vanishing off-diagonal matrix elements are taken to be (in cm^{-1})

$$\langle m-1, n+1|\hat{H}_{\mathrm{HCAO}}|m,n\rangle = \lambda\sqrt{m(n+1)} \tag{17}$$

and

$$\langle m+1, n-1|\hat{H}_{\mathrm{HCAO}}|m,n\rangle = \lambda\sqrt{(m+1)n} \tag{18}$$

with no off-diagonal matrix elements between levels having different values of $V = m + n$. There are three parameters in the HCAO model: ω_M, x_M, and λ. The deviation of the term values from those of the ideal local mode oscillator (i.e., those for $\lambda = 0$) will be small if λ is small in comparison with x_M since x_M governs the separation of the states coupled by λ. The parameter λ is the sum of potential energy and kinetic energy intermode coupling terms. From Eqs. (39), (40), and (68) of Ref. [11], we obtain the following expression for λ as a function of ρ ($=\pi - \alpha$) for the $\widetilde{X}$ state of the PH_2 molecule:

$$\lambda(\rho) = -\left(\frac{x_M}{\omega_M}\right)F_{13}^{(-)}(\rho) + \left(\frac{\omega_M}{2}\right)\left(\frac{m_H}{m_H + m_P}\right)\cos\rho, \tag{19}$$

where $F_{13}^{(-)}(\rho)$ is the quadratic intermode potential energy coupling parameter for the $\widetilde{X}$-state (see Eq. (2)), and we neglect the difference between $\bar{\rho}$ and ρ. In Eq. (44) of Ref. [11] $F_{13}^{(-)}(\rho)$ is called $C_{rr'}$. From Eq. (19) we see that the HCAO parameter λ, which is the expectation value $\langle v_2|\lambda(\rho)|v_2\rangle$, will be small compared to x_M if there is a heavy central atom, an equilibrium bond angle α close to 90°, and if the effective intermode potential energy coupling parameter $F_{13}^{(-)}$ (the expectation value $\langle v_2|F_{13}^{(-)}(\rho)|v_2\rangle$) is small compared to ω_M. This is the case for $\widetilde{X}$-state PH_2.

The ($N = 0, J = 1/2$) term values obtained from the RENNER program for $\widetilde{X}$-state PH_2 are organized in columns headed RENNER, for $v_2 = 0$, 1, 2, and 3, in Table 5. We obtain values for the HCAO parameters ω_M, x_M, and λ, for each value of v_2, by adjusting them so that diagonalization of the $(m + n) = 1$ and 2 HCAO matrices (with matrix elements given by Eqs. (15), (17), and (18)) reproduces the $(mn^{\pm}) = (10^+)$, (10^-), and (20^+) term values. The parameter values are given in Table 5. We see that λ is small in comparison with x_M. Diagonalizing the HCAO Hamiltonian matrices using those parameter values gives the term values listed under the headings HCAO in Table 5.

Looking under the RENNER headings in Table 5 we find two important results: the first is that the stretching term values occur in close-lying pairs characteristic of a local mode oscillator. The second is that the only significant change in the stretching energy levels caused by bending excitation is the difference $E(10^-;v_2) - E(10^+;v_2)$ (for $v_2 = 0$ this is $\omega_3 - \omega_1$); this difference changes

Table 5
The lowest 10 stretching vibrational term values (in cm^{-1}) in the $\widetilde{X}$ state of PH_2 as a function of v_2

($mn^{\pm}$)	$v_2 = 0$		$v_2 = 1$		$v_2 = 2$		$v_2 = 3$	
	RENNER	HCAO	RENNER	HCAO	RENNER	HCAO	RENNER	HCAO
(21^-)	6855.4	6856.1	6790.9	6792.7	6730.0	6732.2	6672.1	6672.9
(21^+)	6849.0	6845.9	6793.8	6791.5	6745.4	6742.4	6702.8	6696.8
(30^-)	6679.9	6682.2	6625.3	6623.7	6538.5	6567.9	6487.3	6510.7
(30^+)	6680.3	6682.2	6625.3	6623.7	6540.8	6567.9	6489.4	6510.7
(11^+)	4624.5	4623.8	4584.7	4584.2	4548.4	4548.2	4516.9	4515.4
(20^-)	4538.5	4539.2	4498.9	4500.0	4461.3	4463.3	4423.7	4427.3
(20^+)	4538.9	4538.9	4500.0	4500.0	4463.0	4463.0	4425.7	4425.7
(10^-)	2314.3	2314.3	2292.4	2292.4	2271.4	2271.4	2250.9	2250.9
(10^+)	2309.2	2309.2	2291.8	2291.8	2276.5	2276.5	2262.9	2262.9
(00^+)	0.0	0.0	(1105.5)[a]	0.0	(2197.4)[a]	0.0	(3277.7)[a]	0.0
ω_M (cm^{-1})		2396.04		2376.29		2358.54		2343.36
x_M (cm^{-1})		−42.15		−42.10		−42.30		−43.23
λ (cm^{-1})		−2.55		−0.30		+2.55		+6.00
$F_{13}^{(-)}$ (cm^{-1})		−212		−89		+66		+248

Those under the heading RENNER are from using the RENNER program, and those under the heading HCAO are obtained by diagonalizing the HCAO Hamiltonian matrix using the parameter values ω_M, x_M, and λ indicated (see text).

[a] Term values of the ($0,v_2,0$) levels relative to (0,0,0).

from $+5.1\ \mathrm{cm}^{-1}$ for $v_2 = 0$ to $-12.0\ \mathrm{cm}^{-1}$ for $v_2 = 3$. By comparing the results under the headings HCAO with those under the headings RENNER, for each v_2 value, we see that the simple three-parameter HCAO Hamiltonian model successfully reproduces the term value patterns. Further, the significant change in $E(10^-;v_2) - E(10^+;v_2)$ that occurs with change in v_2 results in a significant change in the coupling parameter λ with v_2; there are only relatively small changes in ω_M and x_M caused by excitation of the bending mode.

Using the values of λ, ω_M, and x_M from the local mode fitting, and determining the expectation value of $\cos\rho$ for each values of v_2 using the wavefunctions from the RENNER program, we can use Eq. (19) to derive the values of the $F_{13}^{(-)}$ for each value of v_2. The values are given at the bottom of Table 5. From Eq. (4) we have

$$F_{13}^{(-)}(\rho) = f_{13}^{(0)} + \sum_{i=1}^{3} f_{13}^{(i,-)}(1-\cos\rho)^i, \tag{20}$$

where the values of the $\widetilde{X}$-state potential parameters $f_{13}^{(0)}$ are given in Table 1. In Fig. 8 we plot $F_{13}^{(-)}(\rho)$ as a function of ρ and we plot the square of the $v_2 = 0$ and 3 wavefunctions $f(\rho)$. $F_{13}^{(-)}(\rho)$ changes sign at $\rho = 90.42°$ and, since the equilibrium value of ρ is close to this value, the expectation value $F_{13}^{(-)}$ will be small and will be a sensitive function of v_2. Using the wavefunctions from the RENNER program we obtain $F_{13}^{(-)}$ values of -85, -29, $+26$, and $+79\ \mathrm{cm}^{-1}$ for $v_2 = 0$ to 3, respectively; it is small compared to ω_M. This shows why $F_{13}^{(-)}$ is small and how its sign change as v_2 increases (see Table 5) comes about. Considering the approximations inherent in the HCAO model, in Eq. (19), and in replacing $\bar{\rho}$ by ρ, it would be fortuitous if better agreement with the value of $F_{13}^{(-)}$ derived by fitting to the term values were obtained.

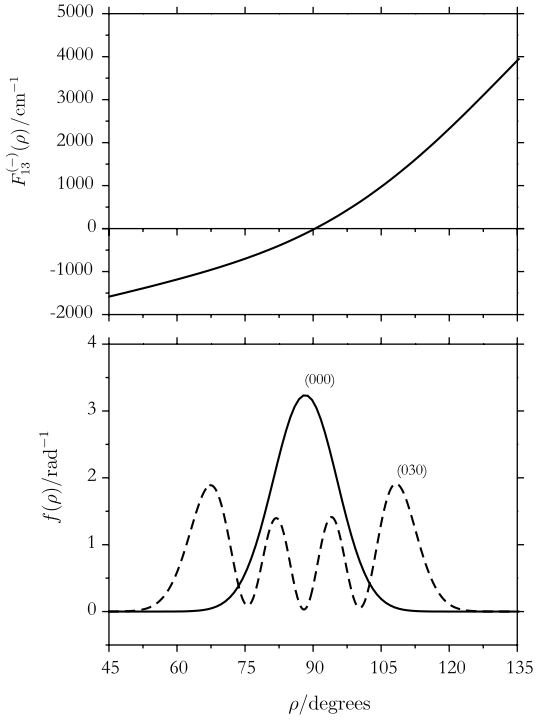

Fig. 8. The ρ dependence of $F_{13}^{(-)}(\rho)$ and of the normalized probability density $f(\rho)$ for the states $v_2 = 0$ and 3.

A similar analysis of the stretching term values for $v_2 = 0$ $\widetilde{A}$-state PH_2 gives $\omega_M = 2526.15\ \mathrm{cm}^{-1}$, $x_M = -49.50\ \mathrm{cm}^{-1}$ and $\lambda = -46.31\ \mathrm{cm}^{-1}$, with very similar parameter values for the higher bending states. For $\widetilde{A}$-state PH_2 the stretching term values have a pattern that is close to the normal mode situation, and λ is not small in comparison to x_M.

As is to be expected, since they do no affect the stretching dynamics, the stretching energy levels are hardly affected by increasing A_{SO} to $800\ \mathrm{cm}^{-1}$ or by reducing $T_e(\widetilde{A})$ to $1000\ \mathrm{cm}^{-1}$; the latter change increases the action of the Renner effect.

5. Intensities

In Ref. [1] the $\widetilde{A}(0,4,0) \rightarrow \widetilde{X}$ (v_1, v_2,v_3) fluorescence spectrum of PH_2 was measured, and the positions of the

Table 6
Term values (T, in cm^{-1}) of the vibrational levels of the $\widetilde{X}^2B_1$ ground electronic state as calculated using the potential surface of Table 1, and relative intensities (I) of fluorescence from the (040) $\widetilde{A}^2A_1$ level, as calculated using the dipole and transition moment surfaces of Table 2

($v_1v_2v_3$)	T			I		
	obs.[a]	calc.	Δ	obs.[a]	calc.[b]	calc.[c]
(000)	0	0	0	145	238	234
(010)	1102(3)	1105	−3	9	4.8	4.5
(020)	2195(3)	2197	−2	47	56	56
(100)	2298(3)	2309	−11	13	5	9.6
(001)		2314			<0.1	<0.1
(030)	3275(3)	3278	−3	32	32	32
(110)	3390(3)	3397	−7	5	3.1	3.8
(011)		3398			0.3	0.1
(040)		4347			0.3	0.2
(021)		4469			<0.1	<0.1
(120)		4474			0.1	0.5
(101)		4539			<0.1	<0.1
(200)		4540			0.1	0.2
(002)		4626			<0.1	<0.1
(050)	5404(5)	5407	−3	15	15	15.2
(031)		5528			<0.1	<0.1
(130)	5524(5)	5541	−17	7	3.4	4.7
(111)		5606			<0.1	<0.1
(210)	5636(5)	5607	29	10	0.3	0.4
(012)		5692			<0.1	0.1
(060)	6458(5)	6457	1	8	10	11.5
(041)		6578			<0.1	<0.1
(140)	6586(5)	6598	−12	4	2.5	2.7
(121)		6661			<0.1	<0.1
(220)		6663			0.2	0.2
(300)		6685			<0.1	<0.1
(201)		6685			<0.1	<0.1
(022)		6749			<0.1	<0.1
(102)		6855			<0.1	<0.1
(003)		6858			<0.1	<0.1

[a] Observed data from Ref. [1].
[b] Calculated relative intensities from Ref. [1]. Obtained using the transition moment from Ref. [21] and scaled so that $I(030) = 32$.
[c] Present relative intensity calculation which is scaled so that $I(030) = 32$. The corresponding calculated line strength value is 0.03062 D^2.

lines were calculated using the RENNER program with the potentials of Table 1. We also calculated the relative intensities, as a function of (v_1,v_2,v_3) in the $\widetilde{X}$ state, using the RENNER program with bending transition moment parameters that we derived from the results in Ref. [21]. These previously calculated relative intensities are given in the penultimate column of Table 6. We have now recalculated these relative intensities using our newly determined dipole moment and transition moment surfaces. The results are given in the last column of Table 6. Although we calculate the absolute values of the transition moments to be about 7.5 times larger than the values reported in Ref. [21], the variation with bending angle is very similar and hence the relative intensities are little changed by our new calculation. The measured values of the lifetimes of $\widetilde{A}$-state vibrational levels [22,23] support our absolute value of the transition moments. The new calculation does not resolve the problem of the rather high experimental relative intensity of 10 for the fluorescence down to the (210) level, where the intensities are scaled so that intensity of the fluorescence down to the (030) level is 32; our new calculation gives only 0.4 for the relative intensity down to the (210) level.

We can use the RENNER computer program to simulate absorption spectra within or between the $\widetilde{X}$ and $\widetilde{A}$ states of the PH_2 molecule. Table 7 gives the linestrength and absorption intensity (assuming a Boltzmann distribution at 300 K) for the $\Delta J = \Delta N = +1$ transition from the ground rovibronic level, for which $J = 1/2$ and $N = 0$, into each excited stretching level up to the $V = 5$ manifold. For each of the rovibronic transitions we give also the vibronic transition moment square $|T_{if}|^2$ (defined in Ref. [6]) for the vibronic band that the transition belongs to. In the absence of Coriolis and spin–orbit interaction, the line strength of an individual rovibronic transition is the product of the transition moment square and a rotational factor related to the Hönl-London factors (see, for example, Ref. [29]) for linear molecules and symmetric tops.

In the pure local mode situation only the lowest two states [i.e., the states $(N0^{\pm})$] within each stretching manifold have non-zero transition intensity in absorption from the ground state [11]. Table 7 shows that these states indeed have the largest values of the vibronic transition moment square $|T_{if}|^2$. For $N = 2$, 3, or 4, the $(N0^{\pm})$ states have $|T_{if}|^2$-values about 100 times larger than those of the other vibrational states in the same stretching manifold. The line strength values S_{if} and absorption intensity values I_{if} for the selected rovibronic transition (Table 7) to the states in these manifolds show the same trend; obviously the line strengths of these transitions is essentially given by the vibronic transition moment square. The breakdown of the local mode approximation gives some intensity to stretching states other than the $(N0^{\pm})$ states in each manifold. For the manifold of states $(nm\pm)$ with $n + m = 5$, (50+) and (50−) have the largest values of $|T_{if}|^2$, but the state (41+) has a value of $|T_{if}|^2$ which is only about seven times smaller than that of (50+). Also, for the states with $n + m = 4$ or 5 there is no simple correlation between $|T_{if}|^2$ and S_{if}. Clearly, for the very weak transitions in

Table 7
The wavenumber v_{if}, linestrength S_{if}, absorption intensity I_{if}[a], and vibronic transition moment square $|T_{if}|^2$ (see text) of the $\Delta J = \Delta N = +1$ transition from the ground rovibronic state $[J = 1/2, N_{K_aK_c} = 0_{00}, (v_1,v_2,v_3) = (0,0,0)]$ to each of the stretching excited states, vibrationally labeled in local mode fashion as $(nm\pm)$, up to the states having $(n + m) = 5$

Upper state					v_{if} (cm^{-1})	S_{if}/D^2	I_{if} (cm mol^{-1})	$\lvert T_{if}\rvert^2$/D^2
J	N	K_a	K_c	$(nm\pm)$				
3/2	1	0	1	(32−)	11239.8	6.35×10^{-13}	1.02×10^{-5}	1.31×10^{-14}
3/2	1	1	1	(32+)	11235.6	4.66×10^{-12}	7.49×10^{-5}	2.20×10^{-12}
3/2	1	0	1	(41−)	11059.7	1.37×10^{-11}	2.17×10^{-4}	1.04×10^{-12}
3/2	1	1	1	(41+)	11053.8	1.89×10^{-11}	2.99×10^{-4}	2.81×10^{-11}
3/2	1	1	1	(50+)	10675.5	2.36×10^{-11}	3.60×10^{-4}	1.94×10^{-10}
3/2	1	0	1	(50−)	10673.9	3.04×10^{-9}	4.64×10^{-2}	2.04×10^{-9}
3/2	1	1	1	(22+)	9095.2	4.50×10^{-12}	5.85×10^{-5}	4.14×10^{-12}
3/2	1	1	1	(31+)	9007.0	6.92×10^{-12}	8.91×10^{-5}	8.24×10^{-15}
3/2	1	0	1	(31−)	9004.2	1.41×10^{-10}	1.82×10^{-3}	2.60×10^{-11}
3/2	1	1	1	(40+)	8734.4	9.42×10^{-10}	1.18×10^{-2}	1.21×10^{-9}
3/2	1	0	1	(40−)	8732.5	5.08×10^{-9}	6.34×10^{-2}	2.10×10^{-9}
3/2	1	0	1	(21−)	6867.2	7.44×10^{-10}	7.30×10^{-3}	1.21×10^{-10}
3/2	1	1	1	(21+)	6861.7	6.44×10^{-10}	6.31×10^{-3}	1.96×10^{-10}
3/2	1	1	1	(30+)	6693.2	1.27×10^{-7}	1.21	5.80×10^{-8}
3/2	1	0	1	(30−)	6691.7	4.55×10^{-8}	4.35×10^{-1}	1.61×10^{-8}
3/2	1	1	1	(11+)	4637.5	3.07×10^{-7}	2.03	1.04×10^{-7}
3/2	1	1	1	(20+)	4551.9	2.66×10^{-5}	1.73×10^{2}	1.35×10^{-5}
3/2	1	0	1	(20−)	4550.4	3.05×10^{-5}	1.98×10^{2}	1.60×10^{-5}
3/2	1	0	1	(10−)	2326.4	1.24×10^{-2}	4.13×10^{4}	9.99×10^{-3}
3/2	1	1	1	(10+)	2322.4	1.17×10^{-2}	3.88×10^{4}	4.08×10^{-3}

[a] Assuming a Boltzmann distribution with a temperature of 300 K.

these states, Coriolis and spin–orbit interaction have a more significant relative effect in spoiling the local mode approximation for the intensities.

With the aim of assisting in the assignment of experimental PH_2 spectra, we give in Tables 8–10 the zero-order subband origins $\nu_K^{(0)}$ and vibronic transition moment squares $|T_{if}|^2$ for a selection of vibronic bands: Table 8 lists values for transitions from the $\widetilde{X}(0,0,0)$ state to $\widetilde{X}(v_1,v_2,v_3)$ states with $v_2>0$; Table 9 lists values for hot bands within the $\widetilde{X}$ state; and Table 10 gives values for $\widetilde{A}\leftarrow\widetilde{X}$ transitions. The quantity $\nu_K^{(0)}$ is the approximate transition wavenumber of a hypothetical transition with $N=K'\leftarrow K''$; it corresponds to the difference between two eigenvalues of an approximate rovibronic Hamiltonian obtained by neglecting, in the complete rovibronic Hamiltonian, the terms describing end-over-end rotation and spin–orbit interaction (see Ref. [6]). The lower-state energies $E_{K''}^{(0)}$ in Table 9 are eigenvalues of the approximate rovibronic Hamiltonian.

6. Summary and discussion

We have calculated the term values of highly excited rotational and vibrational levels of $\widetilde{X}$-state PH_2, and calculated spectra involving levels of both the $\widetilde{X}$ and $\widetilde{A}$

Table 8
Calculated zero-order subband origins $\nu_K^{(0)}$[a] and vibronic transition moment squares $|T_{if}|^2$ for transitions $\widetilde{X}(v_1,v_2,v_3)^K\leftarrow\widetilde{X}(0,0,0)^0$ of PH_2

$(v_1,v_2,v_3)^K$	$\nu_K^{(0)}$ (cm^{-1})	$\lvert T_{if}\rvert^2$/D^2
$(0,0,0)^1$	13.31	1.49×10^{-1}
$(0,1,0)^1$	1118.93	3.08×10^{-3}
$(0,2,0)^1$	2211.18	1.34×10^{-4}
$(0,3,0)^1$	3291.78	1.12×10^{-7}
$(0,1,1)^0$	3397.70	1.21×10^{-5}
$(1,1,0)^1$	3410.45	3.71×10^{-5}
$(0,4,0)^1$	4361.82	1.07×10^{-7}
$(0,2,1)^0$	4468.67	2.38×10^{-6}
$(1,2,0)^1$	4487.40	2.37×10^{-6}
$(0,5,0)^1$	5421.89	6.21×10^{-8}
$(0,3,0)^0$	5528.48	2.94×10^{-7}
$(1,3,0)^1$	5554.39	1.32×10^{-7}
$(1,1,1)^0$	5604.10	2.68×10^{-6}
$(2,1,0)^1$	5618.42	4.24×10^{-8}
$(0,1,2)^1$	5703.04	4.81×10^{-8}
$(0,6,0)^1$	6472.27	7.29×10^{-9}
$(0,4,1)^0$	6577.90	6.60×10^{-9}
$(1,4,0)^1$	6611.81	5.69×10^{-8}
$(1,2,1)^0$	6658.46	1.20×10^{-7}
$(2,2,0)^1$	6673.52	7.91×10^{-9}
$(0,2,2)^1$	6759.33	1.12×10^{-8}
$(0,7,0)^1$	7513.07	2.87×10^{-13}
$(0,5,1)^0$	7617.21	1.39×10^{-9}
$(1,5,0)^1$	7659.27	3.37×10^{-9}
$(1,3,1)^0$	7701.09	1.10×10^{-7}
$(3,1,0)^1$	7716.67	8.26×10^{-9}
$(2,1,1)^0$	7730.41	1.32×10^{-7}
$(3,1,0)^1$	7743.59	8.16×10^{-10}
$(0,3,2)^1$	7808.12	1.39×10^{-9}
$(0,1,3)^0$	7895.99	6.03×10^{-10}
$(1,1,2)^1$	7911.76	1.17×10^{-9}

[a] The quantity $\nu_K^{(0)}$ is the approximate transition wavenumber of a transition with $N=K'\leftarrow K''$ (see text).

Table 9
Calculated zero-order subband origins $\nu_K^{(0)}$[a], approximate lower state term values E_0''[b] and vibronic transition moment squares $|T_{if}|^2$ for hot vibrational transitions $\widetilde{X}(v_1',v_2',v_3')^{K'}\leftarrow\widetilde{X}(v_1'',v_{2''},v_{3''})^0$ of PH_2

$(v_1',v_2',v_3')^{K'}$	$(v_1'',v_2'',v_3'')^0$	E_0'' (cm^{-1})	$\nu_K^{(0)}$ (cm^{-1})	$\lvert T_{if}\rvert^2$/D^2
$(0,2,0)^1$	$(0,1,0)^0$	1105.34	1105.84	0.0059
$(0,1,1)^0$	$(0,1,0)^0$	1105.34	2292.36	0.0097
$(1,1,0)^1$	$(0,1,0)^0$	1105.34	2305.10	0.0040
$(0,3,0)^1$	$(0,2,0)^0$	2197.30	1094.48	0.0084
$(0,2,1)^0$	$(0,2,0)^0$	2197.30	2271.36	0.0093
$(1,2,0)^1$	$(0,2,0)^0$	2197.30	2290.09	0.0039
$(1,1,0)^1$	$(1,0,0)^0$	2309.05	1101.40	0.0029
$(1,0,1)^0$	$(1,0,0)^0$	2309.05	2229.11	0.0106
$(2,0,0)^1$	$(1,0,0)^0$	2309.05	2242.45	0.0046
$(0,0,2)^1$	$(1,0,0)^0$	2309.05	2328.04	0.0037
$(0,1,1)^1$	$(0,0,1)^0$	2314.14	1096.87	0.0028
$(2,0,0)^0$	$(0,0,1)^0$	2314.14	2224.49	0.0096
$(1,0,1)^1$	$(0,0,1)^0$	2314.14	2236.87	0.0042
$(0,0,2)^0$	$(0,0,1)^0$	2314.14	2310.08	0.0110
$(0,4,0)^1$	$(0,3,0)^0$	3277.59	1084.23	0.0104
$(0,5,0)^1$	$(0,3,0)^0$	3277.59	2144.30	0.0014
$(0,3,1)^0$	$(0,3,0)^0$	3277.59	2250.89	0.0090
$(1,3,0)^1$	$(0,3,0)^0$	3277.59	2276.80	0.0037
$(1,2,0)^1$	$(1,1,0)^0$	3397.06	1090.33	0.0055
$(1,1,1)^0$	$(1,1,0)^0$	3397.06	2207.04	0.0102
$(2,1,0)^1$	$(1,1,0)^0$	3397.06	2221.36	0.0040
$(0,1,2)^1$	$(1,1,0)^0$	3397.06	2305.98	0.0042
$(0,2,1)^1$	$(0,1,1)^0$	3397.70	1084.56	0.0054
$(2,1,0)^0$	$(0,1,1)^0$	3397.70	2207.59	0.0102
$(1,1,1)^1$	$(0,1,1)^0$	3397.70	2219.52	0.0040
$(0,1,2)^0$	$(0,1,1)^0$	3397.70	2292.22	0.0097

Only transitions for which $|T_{if}|^2>0.0001$ D^2 are listed.

[a] The quantity $\nu_K^{(0)}$ is the approximate transition wavenumber of a transition with $N=K'\leftarrow K''$ (see text).

[b] The quantity E_0'' is the term value of the lower state obtained when the contributions from end-over-end rotation and spin–orbit interaction are neglected (see text).

Table 10
Calculated zero-order subband origins $\nu_K^{(0)}$[a]

$(v_1,v_2,v_3)^1$	$\nu_K^{(0)}$ (cm^{-1})	$\lvert T_{if}\rvert^2$/D^2
$(0,4,0)^1$	22064.23	3.32×10^{-2}
$(0,3,0)^1$	21133.39	3.18×10^{-2}
$(0,5,0)^1$	22996.73	2.79×10^{-2}
$(0,2,0)^1$	20197.63	2.27×10^{-2}
$(0,6,0)^1$	23942.40	2.03×10^{-2}
$(0,7,0)^1$	24913.73	1.31×10^{-2}
$(0,1,0)^1$	19254.06	1.08×10^{-2}
$(0,0,0)^1$	18301.51	2.60×10^{-3}
$(1,2,0)^1$	22554.60	4.08×10^{-4}
$(1,3,0)^1$	23479.40	3.56×10^{-4}
$(1,1,0)^1$	21622.52	2.90×10^{-4}
$(1,4,0)^1$	24399.73	2.44×10^{-4}
$(1,0,0)^1$	20681.91	9.48×10^{-5}
$(2,0,0)^1$	23000.36	5.43×10^{-5}
$(2,1,0)^1$	23928.33	4.06×10^{-5}
$(2,2,0)^1$	24848.25	1.76×10^{-5}
$(0,2,2)^1$	25047.16	5.59×10^{-6}
$(0,1,2)^1$	24130.61	2.65×10^{-6}
$(0,0,2)^1$	23205.24	7.11×10^{-7}

[a] The quantity $\nu_K^{(0)}$ is the approximate transition wavenumber of a transition with $N=K'\leftarrow K''$ (see text). and vibronic transition moment squares $|T_{if}|^2$ for the vibronic transitions $\widetilde{A}(v_1,v_2,v_3)^1\leftarrow\widetilde{X}(0,0,0)^0$ of PH_2.

electronic states of the molecule. These states form a Renner-degenerate pair, and to make the calculations we have used the computer program RENNER [4–6]. We have used $\widetilde{X}$ and $\widetilde{A}$ state potential surfaces that we previously derived [1], and have calculated dipole moment surfaces, and the $\widetilde{A}$–$\widetilde{X}$ transition moment surface, using *ab initio* methods. The $\widetilde{X}$ state of PH_2 has an equilibrium angle that is close to 90°, the central atom is much heavier than the terminal atoms, and intermode mixing is not very strong. Because of these three facts the rovibrational energy level pattern exhibits 4-fold clusters at high angular momentum, and the stretching energy levels conform closely to those of a local mode oscillator; we have studied these two phenomena by calculation in $\widetilde{X}$-state PH_2.

This is the first study of 4-fold energy level clustering in a non-singlet state. We have determined how spin–orbit coupling, the Renner effect and excitation of the v_2 bending mode influence the formation of the clusters. We have found that, for the $\widetilde{X}$ doublet state of PH_2, the F_1 and F_2 levels each form 4-fold clusters whose separation increases with the extent of the spin–orbit coupling between the $\widetilde{X}$ and $\widetilde{A}$ states (see Table 3). If there were no such spin–orbit coupling then an 8-fold energy level cluster would form. The 4-fold clusters begin to form at around $N = 15$, as is predicted by semiclassical theory, and they are well developed at $N = 30$ in our calculations. The cluster splitting is significantly reduced in the F_1 and F_2 levels by excitation of the bending vibration v_2, as can be seen in Table 4. The fact that cluster formation is enhanced by excitation of the bending vibration can be understood if we realize that the extent of cluster formation in a particular vibrational state depends on how easily a molecule in that state can be deformed by centrifugal distortion. With increasing bending excitation the zero-order bending wavefunction acquires significant amplitude over an increasingly larger ρ-interval which increases the centrifugal deformability of the state. Experimental studies of $\widetilde{X}$-state PH_2 in levels having high values for both N and K_a have not yet been made; such states might be produced by photodissociation of PH_3 [30], or in flame experiments [31].

We show by calculation that the term values of the stretching vibrational levels in the $\widetilde{X}$ state conform closely to the paired energy level pattern appropriate for a local mode oscillator, and we have calculated how the local mode stretching energy level pattern changes with bending excitation (see Table 5); stretching term values have been calculated in the bending states $v_2 = 0$, 1, 2, and 3. The only significant change in the stretching energy levels caused by bending excitation is the difference $E(10^-;v_2) - E(10^+;v_2)$ which changes from $+5.1\,cm^{-1}$ for $v_2 = 0$ to $-12.0\,cm^{-1}$ for $v_2 = 3$. This is well modeled using the single harmonically coupled anharmonic oscillator (HCAO) coupling parameter λ, which changes significantly as v_2 is excited. The change in λ with bending excitation can be semi-quantitatively accounted for within the HCAO model using the approximate expression for $\lambda(\rho)$ given in Eq. (19) which, in turn, implies a significant change in the effective potential energy coupling parameter $F_{13}^{(-)}$ with v_2 as given at the bottom of Table 5. This change comes about because of the way $F_{13}^{(-)}(\rho)$ varies with ρ according to Eq. (20), and this is shown in Fig. 8.

Using the dipole moment and transition moment surfaces we have recalculated the relative intensities of the vibrational structure in the fluorescence spectrum that has been recorded [1] from the (0,4,0) vibrational level of the $\widetilde{A}$ state. From the results in Table 6 we see that we are still unable to explain the rather high relative intensity of the fluorescence down to the (210) vibrational level of the $\widetilde{X}$ state. We have also calculated the vibronic transition moment squares for selected $\widetilde{X} \leftarrow \widetilde{X}$ and $\widetilde{A} \leftarrow \widetilde{X}$ vibronic bands together with the line-strengths and absorption intensities of individual rovibronic transitions to excited stretching levels within the $\widetilde{X}$ state. These latter results follow the trends predicted by local mode theory.

Acknowledgments

The work of P.J. is supported in part by the Deutsche Forschungsgemeinschaft and the Fonds der Chemischen Industrie, and the work of P.J., W.T., and S.N.Y. was undertaken under the auspices of the Marie Curie Research Training Network QUASAAR "Quantitative Spectroscopy for Atmospheric and Astrophysical Research" financed by the European Commission as contract no. MRTN-CT-2004-512202. We thank Stephan Sauer for helpful discussions concerning the *ab initio* calculations.

References

[1] Z.J. Jakubek, P.R. Bunker, M. Zachwieja, S.G. Nakhate, B. Simard, S.N. Yurchenko, W. Thiel, P. Jensen, J. Chem. Phys. 124 (2006), 094306/1–5.
[2] P. Jensen, T.E. Odaka, W.P. Kraemer, T. Hirano, P.R. Bunker, Spectrochim. Acta 58 (2002) 763–794.
[3] P. Jensen, P.R. Bunker, (Eds.), Computational Molecular Spectroscopy, Wiley, Chichester, England, 2000. See <http://www.chem.uni-wuppertal.de/cms/>.
[4] P. Jensen, M. Brumm, W.P. Kraemer, P.R. Bunker, J. Mol. Spectrosc. 171 (1995) 31–57.
[5] M. Kolbuszewski, P.R. Bunker, P. Jensen, W.P. Kraemer, Mol. Phys. 88 (1996) 105–124.
[6] G. Osmann, P.R. Bunker, P. Jensen, W.P. Kraemer, Chem. Phys. 225 (1997) 33–54.
[7] I.N. Kozin, S.P. Belov, O.L. Polyanski, M.Yu. Tretyakov, J. Mol. Spectrosc. 152 (1992) 13–28.
[8] P. Jensen, I.N. Kozin, J. Mol. Spectrosc. 160 (1993) 39–57.
[9] I.N. Kozin, P. Jensen, J. Mol. Spectrosc. 161 (1993) 186–207.
[10] P. Jensen, G. Osmann, I.N. Kozin, in: D. Papoušek (Ed.), Vibration–Rotational Spectroscopy and Molecular Dynamics, World Scientific, Singapore, 1997.
[11] P. Jensen, Mol. Phys. 98 (2000) 1253–1285.
[12] G.W. Hills, A.R.W. McKellar, J. Chem. Phys. 71 (1979) 1141–1149.

[13] P.R. Bunker, P. Jensen, Molecular Symmetry and Spectroscopy, second ed., NRC Research Press, Ottawa, Canada, 1998, See <http://www.nrc.ca/cgi-bin/cisti/journals/rp/rp2_book_e?mlist1_90/>.
[14] A. Alijah, G. Duxbury, J. Opt. Soc. Am. B 11 (1994) 208–218.
[15] MOLPRO is a package of *ab initio* programs written by H.-J. Werner and P.J. Knowles, with contributions from R.D. Amos, A. Bernhardsson, A. Berning, P. Celani, D.L. Cooper, M.J.O. Deegan, A.J. Dobbyn, F. Eckert, C. Hampel, G. Hetzer, T. Korona, R. Lindh, A.W. Lloyd, S.J. McNicholas, F.R. Manby, W. Meyer, M.E. Mura, A. Nicklass, P. Palmieri, R.M. Pitzer, G. Rauhut, M. Schütz, H. Stoll, A.J. Stone, R. Tarroni, T. Thorsteinsson.
[16] H.-J. Werner, P.J. Knowles, J. Chem. Phys. 89 (1988) 5803–5814.
[17] P.J. Knowles, H.-J. Werner, Chem. Phys. Lett. 145 (1988) 514–522.
[18] R.A. Kendall, T.H. Dunning, R.J. Harrison, J. Chem. Phys. 96 (1992) 6796–6806.
[19] H.L. Woodcock, S.S. Wesolowski, Y. Yamaguchi, H.F. Schaefer III, J. Phys. Chem. A 105 (2001) 5037–5045.
[20] P. Jensen, J. Mol. Spectrosc. 132 (1988) 429–457.
[21] M. Perić, R.J. Buenker, S.D. Peyerimhoff, Can. J. Chem. 57 (1979) 2491–2497.
[22] C.N. Xuan, A. Margani, J. Chem. Phys. 93 (1990) 136–146.
[23] C.N. Xuan, A. Margani, J. Chem. Phys. 100 (1994) 7000–7011.
[24] R.N. Dixon, Mol. Phys. 10 (1965) 1–6.
[25] R.N. Dixon, G. Duxbury, D.A. Ramsay, Proc. R. Soc. A 296 (1967) 137–160.
[26] J.-M. Bertou, B. Pascat, H. Guenebaut, D.A. Ramsay, Can. J. Phys. 50 (1972) 2265–2276.
[27] M.S. Child, R.T. Lawton, Faraday Discuss. Chem. Soc. 71 (1981) 273–285.
[28] O.S. Mortensen, B.R. Henry, M.A. Mohammadi, J. Chem. Phys. 75 (1981) 4800–4808.
[29] P.R. Bunker, P. Jensen, Fundamentals of Molecular Symmetry, IOP Publishing, Bristol, 2004.
[30] D. Baugh, B. Koplitz, Z. Xu, C. Wittig, J. Chem. Phys. 88 (1988) 879–887.
[31] B. Pascat, J.-M. Bertou, J.-C. Prudhomme, H. Guenebaut, D.A. Ramsay, J. Chim. Phys. 65 (1968) 2022–2029.